NUMERICAL STUDY OF NON-EQUILIBRIUM PROCESSES IN HIGH ENTHALPY FLOWS

E. SCHALL, Y. BURTSCHELL AND D. ZEITOUN

Lab. IUSTI/SETT (URA CNRS 1168), Dept. MHEQ, Université de Provence - St Jérôme, 13397 Marseille Cedex 20, France

ABSTRACT

Non-equilibrium hypersonic viscous flows with high enthalpy conditions have been computed with an implicit time-dependent finite-difference scheme. This scheme accounts for both chemical and vibrational non-equilibrium processes in air flow around a hemispherical cylindrical body. The air was assumed to decompose into the following five species N, O, NO, N_2 and O_2 and only the two diatomic species N_2 and O_2 are taken in thermal non-equilibrium. A range of Mach number from 14 to 18 has been investigated. The numerical results have been compared with those obtained by other workers and are in agreement with ballistic range data concerning the standoff shock distance at $M = 15.3$. The computed heat flux wall follows the trends of the experiments with an under prediction increasing with the Mach number. The influence of the thermal non-equilibrium assumption on the computed standoff shock distance is investigated.

KEY WORDS   Hypersonic air flow   Mach number   Non-equilibrium flow

INTRODUCTION

A high velocity flow around a body leads to the formation of a strong bow shock wave. An important transfer of the high kinetic energy to the internal energy modes of the gas takes place through this shock wave. This transfer causes a very strong increase in temperature and, therefore, significant modifications of the composition and of the internal energy distribution of the gas in the nose region. Subsequently, the state of the gas continue to change due to the expansion of the flow along the body wall. These transformations are governed by physico-chemical non-equilibrium processes which can induce important variations of the thermodynamical quantities of the gas flow and of the wall heat flux transfer[1].

To treat these high-temperature conditions, the air is usually considered as a mixture of monoatomic and diatomic species, whose number and internal states depend on the physico-chemical processes being taken into account[2].

In connection with hypersonic flight projects, the study of such flows has renewed an important development during the last several years[3-5]. Owing to the difficulty of operating experimental facilities in the requested conditions, most of the works are resorting to the numerical simulation of high temperature flows with a more-or-less complex modelling of the non-equilibrium processes involved[5].

Within the framework of viscous flow computations, non-equilibrium chemistry assuming thermal equilibrium is often considered for a model of air mixture[6]. This model assumes a total of seventeen chemical reactions, whose reaction rates and equilibrium constants given by Park[7].

When thermal non-equilibrium is taken into account, a single vibrational temperature model is employed with vibration-dissociation coupling, modelled according to the empirical relationship also proposed by Park[7].

More recently, numerical approaches have been developed embedding multi-vibrational temperature models[8,9]. But the validation of such physical models and numerical approaches is still in progress currently.

The subject of the present work is a numerical study of a dissipative air flow in chemical and thermal non-equilibrium around an axisymmetric body at high upstream Mach number, aiming to put into evidence the influence of the non-equilibrium processes on the flowfield parameters. The gas air modelled as a reactive mixture composed of the five following species: N, O, NO, N_2 and O_2 Park's model is used for describing the chemical reactions[2]. The diatomic species N_2 and O_2 are in thermal non-equilibrium and NO is chosen to be in a thermal equilibrium state[10]. The harmonic oscillator assumption is used and the vibrational exchanges take into account only the translation–vibration transfer through the Laudau–Teller theory[11]. A global relaxation time models the exchanges of the molecules with the other species of the mixture[3]. The ionization of atoms has been neglected in the chosen Mach number range.

This non-equilibrium flow is described by a system of ten equations. Owing to the stiffness of the source terms, explicit numerical methods are out of question[12]. In order to solve this system, an implicit finite difference method, following MacCormack[13], is implemented. This method is based on a predictor-corrector scheme, with second order accuracy. In the implicit operator, an Eulerian non-dissipative flux-splitting technique[14] is used. After discretization, the block-pentadiagonal matrix system is solved with a Gauss–Siedel line relaxation method. This numerical approach has been successfully used for describing the non-equilibrium internal flowfield in hypersonic nozzles[15].

Several computational results, for high Mach number flows around axisymmetric sphere-cylinder bodies, are presented. The first one, at Mach number 15.35, corresponds to Lobbs experiments[16]. This case has been computed by several authors[9,14,17]. The following cases correspond to data from the experimental work by Rose *et al.*[18]. In this work, conditions at freestream Mach numbers of 14, 16, 18 and at an altitude of 37 Km are selected. For these last three cases, a code-to-code comparison is also made with a recent paper of Josyula and Shang[8] in which Roe flux-difference split scheme is used. These authors take also into account a thermal non-equilibrium assumption for the NO molecule.

GOVERNING EQUATIONS

In a cylindrical coordinate system, the axisymmetric conservative equations for an air mixture in a chemical and thermal non-equilibrium state are the Navier–Stokes equations with in addition, the mass evolution equations for each species and those for the vibrational energy of each diatomic species. These equations can be expressed in vector form as:

$$\frac{\partial U^-}{\partial t} + \frac{\partial (F_e + F_v)}{\partial x} + \frac{\partial (G_e + G_v)}{\partial y} + \frac{1}{y} H_a = \Omega \tag{1}$$

The vector of conservative quantities is given by:

$$U = (\rho_s, \rho u, \rho v, \rho E, \rho_i e_v)^T \tag{2}$$

where ρ_s is the density of each species, the subscript $s = 1, 2, \ldots, 5$ represents the five species N, O, NO, N_2, O_2, or the air mixture and $i = 1, 2$ refers to the diatomic species N_2, O_2, (NO is supposed to be in thermal equilibrium), ρ is the density of the mixture, u and v the components of the velocity V, and ρE is the total energy per unit volume, containing translational, rotational and vibrational energies, the latent chemical energy of the species and the kinetic energy of

directed motion; ρE is given by:

$$\rho E = \sum_{s=1}^{5} \rho_s c_{v_s} T + \sum_{i=1}^{2} \rho_i e_{v_i} + \rho_{NO} e_{v_{NO}} + \sum_{s=1}^{5} \rho_s h_s^{for} + \frac{1}{2}\rho V^2 \tag{3}$$

In (1) the vectors F_e, G_e, F_v and G_v represent, respectively, the Eulerian convective and viscous fluxes, and can be written as follows:

$$F_e + F_v \begin{bmatrix} \rho_s u - \rho D_{sm}\dfrac{\partial Y_s}{\partial x} \\[2mm] \rho u^2 + P - \tau_{xx} \\[2mm] \rho uv - \tau_{xy} \\[2mm] (\rho E + P - \tau_{xx})u - v\tau_{xy} + q_x \\[2mm] \rho_i u e_{vi} - \rho e_{vi} D_{im}\dfrac{\partial Y_i}{\partial x} + q_{vix} \end{bmatrix}, G_e + G_v \begin{bmatrix} \rho_s v - \rho D_{sm}\dfrac{\partial Y_s}{\partial y} \\[2mm] \rho uv - \tau_{xy} \\[2mm] \rho v^2 + P - \tau_{yy} \\[2mm] (\rho E + P - \tau_{yy})v - u\tau_{xy} + q_y \\[2mm] \rho_i v e_{vi} - \rho e_{vi} D_{im}\dfrac{\partial Y_i}{\partial y} + q_{viy} \end{bmatrix}$$

H_a is the axisymmetric vector given by:

$$H_a \begin{bmatrix} \rho_s v - \rho D_{sm}\dfrac{\partial Y_s}{\partial y} \\[2mm] \rho uv - \tau_{xy} \\[2mm] \rho v^2 - \tau_\theta \\[2mm] (\rho E + P - \tau_{yy})v - u\tau_{xy} + q_y \\[2mm] \rho_i v e_{vi} - \rho e_{vi} D_{im}\dfrac{\partial Y_i}{\partial y} + q_{viy} \end{bmatrix}$$

According to Fick's first law of diffusion and to the Stokes hypothesis, the components of the stress tensor and the heat flux vector can be written as follows:
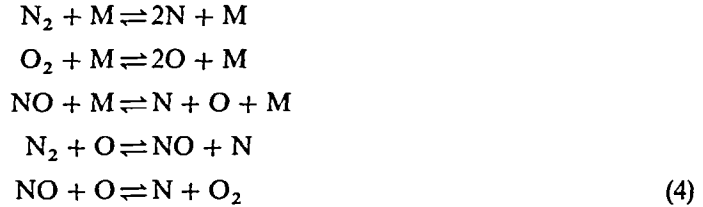
$$\tau_{xx} = \frac{2}{3}\mu_m\left(2\frac{\partial u}{\partial x} - \frac{\partial v}{\partial y} - \frac{v}{y}\right)$$

$$\tau_{xy} = \mu_m\left(\frac{\partial u}{\partial y} + \frac{\partial v}{\partial x}\right)$$

$$\tau_{yy} = \frac{2}{3}\mu_m\left(2\frac{\partial v}{\partial y} - \frac{\partial u}{\partial x} - \frac{v}{y}\right)$$

$$\tau_\theta = 2\mu_m\left(\frac{v}{y} - \frac{\partial v}{\partial y}\right)$$

$$\vec{q} = -k_m\vec{\nabla}T - \sum_{s=1}^{5} h_s \rho D_{sm}\vec{\nabla Y_k} - \sum_{i=1}^{2}(\rho D_{im})Y_i \vec{\nabla e_{vi}}$$

In these expressions, the viscosity μ_m and the thermal conductivity k_m of the mixture are computed by Wilke's mixing rule[18], while the binary diffusion coefficients D_{sm} are given by a Chapman and Cowling empirical formula[20].

As concerns the vector $\Omega_s = (\omega_s, 0, 0, 0, \omega_i)^T$, it contains the chemical source terms ω_s, due to the net rate production of each species, and the vibrational source terms ω_i of the species N_2 and O_2. These terms are the result of the chemical and vibrational non-equilibrium modelling and are described hereafter.

CHEMICAL AND VIBRATIONAL NON-EQUILIBRIUM MODELLING

In the five species air mixture, each species is considered as a perfect gas. The chemical source terms are derived from the reactions that occur between these species, being given by the following 17-reaction scheme:

$$N_2 + M \rightleftharpoons 2N + M$$

$$O_2 + M \rightleftharpoons 2O + M$$

$$NO + M \rightleftharpoons N + O + M$$

$$N_2 + O \rightleftharpoons NO + N$$

$$NO + O \rightleftharpoons N + O_2 \tag{4}$$

with $M = N, O, NO, N_2, O_2$. The first three reactions are dissociation–recombination type and fourth and fifth are exchange reactions. The magnitude of the mass production or removal is obtained from:

$$\omega_s = M_s \sum_r (v''_{sr} - v'_{sr}) \left\{ k_{f,} \prod_s \left(\frac{\rho_s}{M_s} \right)^{v'_{sr}} - k_{b,} \prod_s \left(\frac{\rho_s}{M_s} \right)^{v''_{sr}} \right\} \tag{5}$$

v'_{sr}, v''_{sr} refer to the stoichiometric coefficients, while k_f and k_b are the forward and backward reaction rates, as given by Park[7] and are calculated with translational temperature.

In the vibrational modelling, only vibration–translation energy exchanges are taken into account. The source terms $\omega_{i(T-V)}$ in the vibrational equations are classically described by the Laudau–Teller formulation and are given by:

$$\omega_{i(T-V)} = \frac{\rho_i e^0_{v_i} - \rho_i e_{v_i}}{\tau_i^{VT}} + e_{v_i} \omega_{s=i} \tag{10}$$

with $e^0_{v_i}$ the vibrational energy at equilibrium; since $\omega_{i(T-V)}$ takes into account all the vibrational–translational exchanges, the global relaxation time τ_i^{VT} is expressed as:

$$\frac{1}{\tau_i^{VT}} = \sum_{s=1}^5 \frac{\xi_s}{\tau_{is}^{VT}} \tag{11}$$

where ξ_s is the molar fraction of each species s, and τ_{is}^{VT} is the relaxation time for the exchanges between the diatomic molecules i and any species s; τ_{is}^{VT} has the following general form:

$$p\tau_{is}^{VT} = a_{is} T^{b_{is}} \exp(-c_{is} T^{-1/3} + d_{is}) \tag{12}$$

where a_{is}, b_{is}, c_{is} and d_{is} are constants depending on the colliding species, which can be found in Reference 21 and p is the pressure.

COMPUTATION PROCEDURE

To correctly describe the dissipative effects in the boundary layer which develops along the body wall and the strong flow gradients around the symmetry axis, the mesh distribution must be quite stretched and consequently the time step for integration is very small. In order to overcome this difficulty and others, due to the stiffness of the chemical and vibrational equations, the system of ten governing equations (1) is solved by a strongly implicit finite-difference scheme like that used by MacCormack[13]. The physical domain (x, y) is transformed into a rectangular one (ξ, η) and for each node (i, j) of this domain the system of equations is written at each time

step $(n + 1)\Delta t$ as:

$$\frac{U^{n+1} - U^n}{\Delta t} + \frac{D}{D\xi}(F_e + F_v)^{n+1} + \frac{D}{D\eta}(G_e + G_v)^{n+1} + \frac{1}{y}H_a^{n+1} + H_s^{n+1} = 0 \qquad (18)$$

Φ representing one of the vectors of this equation, it is linearized to yield the expansion:

$$\Phi^{n+1} = \Phi^n + \left(\frac{\partial \Phi}{\partial U}\right)^n \delta U^n \qquad (19)$$

where $(\partial\Phi/\partial U)$ is the Jacobian matrix and $\delta U^n = U^{n+1} - U^n$. Under these conditions, and after using the non-dissipative flux-splitting technique proposed by MacCormack and Candler[22], the system (18) is equivalent to:

$$\left\{I + \Delta t\left(\frac{D_+A_-}{\Delta\xi} + \frac{D_-A_+}{\Delta\xi} + \frac{D^2 S_v}{\Delta\xi^2} + \frac{D_+B_-}{\Delta\eta} + \frac{D_-B_+}{\Delta\eta} + \frac{D^2 R_v}{\Delta\eta^2} + \frac{1}{y}C_a + C_s\right)\right\}\delta U^n = \Delta U^n$$

$$(20)$$

In this equation, D, D_+, D_- are respectively central, forward and backward difference operators, while $A_-, A_+, S_v, B_-, B_+, R_v, C_a, C_s$ are the Jacobian matrices of $F_e^-, F_e^+, F_v, G_e^-, G_e^+, G_v, H_a$, and H_s, C_a contains only the Jacobian of the non-dissipative part of the vector H_a.

After discretization, the system (20) may be written as a pentadiagonal matrix linear system:

$$\hat{B}_{i,j}\delta U_{i,j+1}^n + \bar{A}_{i,j}\delta U_{i,j}^n + \hat{C}_{i,j}\delta U_{i,j-1}^n + \hat{D}_{i,j}\delta U_{i+1,j}^n + \hat{E}_{i,j}\delta U_{i-1,j}^n = \Delta U_{i,j}^n \qquad (21)$$

At each time step, a predictor-corrector scheme is used, and the system (21) is solved by a Gauss–Seidel line or point relaxation method, with alternating sweeps in the backward and forward ξ directions. The conservation vector U is updated by:

$$U_{i,j}^{n+1} = U_{i,j}^n + \delta U_{i,j}^n \qquad (22)$$

The knowledge of vector U allows to obtain the following variables: $\rho_s(s = 1, \ldots, 5)$, $\rho, u, v, e_{t_i}(i = 1, 2)$. After that the temperature is deduced from (3) using a Newton–Raphson iteration, the pressure is found through the state equation of the gas mixture.

Associated to this algorithm, the boundary conditions of the computational domain are given as undisturbed freestream values on the upstream boundary. A zero-extrapolation is imposed for the supersonic downstream boundary. A non-slip condition for the velocity components, zero normal pressure gradient, isothermal and non-catalytic conditions are enforced on the body surface.

In the mesh distribution, the wall is located on the middle of the first mesh in the normal direction.

CONDITIONS OF NUMERICAL SIMULATION

The validation of chemical and thermal non-equilibrium flow computations is rather delicate, due to the scarcity of experimental results. Upstream flow conditions as corresponding to Lobbs[16] and Rose et al.[18] experiments around a hemisphere-cylinder model, have been chosen.

These conditions are reported on the *Table 1*. In each case the freestream gas was composed of 79% N_2 and 21% O_2.

Several authors have used these experimental conditions in order to validate their numerical codes and, so a code-to-code comparison will be also presented, for each case, in the following section.

The mesh distribution is the same for all computational cases and is drawn in *Figure 1*. The number of the mesh points is of (50 × 50) with a refinement near the wall for a better boundary

Table 1   Details of flow conditions

Experiments	M_∞	T_∞ (K)	R_s (mm)	T_w (K)	Re_∞
Lobbs	15.35	293	6.35	1000	14605
Rose *et al.*	18	252	6.6	555.5	12840
Rose *et al.*	16	252	6.6	555.5	11413
Rose *et al.*	14	252	6.6	555.5	9987
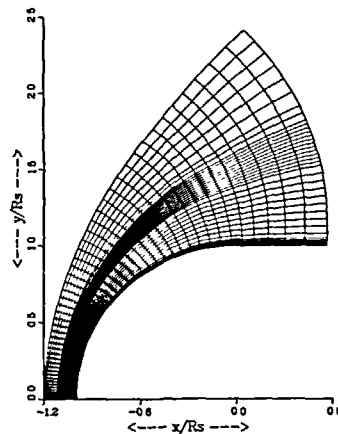
Figure 1   Grid system for hemispherical cylinder

layer capturing, near the symmetry axis for reducing the numerical bulge, and around the shock position. The minimum grid spacing in the radial direction and along the body surface are respectively equal to $\Delta\eta = 0.16 \times 10^{-4}$ and $\Delta\xi = 1 \times 10^{-3}$.

At the initial time, the flow quantities are initialized with an Euler solution in the same freestream conditions. The steady state is obtained after about 3000 iterations when the L2 norm residual drops by more than five order of magnitude. During the convergence procedure the CFL number varies from 1 to 50. The CPU time is equal to 1×10^{-3} sec/pt/iter on a CRAY YMP-2E computer for the complete set of equations. It can be noted that, before the convergence procedure is achieved, the mesh distribution is refined around the shock position and a second and fourth order adaptative dissipation technique[23] is used for preventing oscillations near the shock, as well as for smoothing any high-frequency oscillations. The coefficients associated to this technique are respectively equal to $\varepsilon_2 = 0.65$ and $\varepsilon_4 = 0.04$.

DISCUSSION OF RESULTS

The numerical results are presented in the two following sections. In the first section, the experimental flows conditions of Lobbs are used. Comparisons with the experimental standoff shock position (only this experimental value is given) and with other computational results[3-9], concerning the others quantities, are made.

In the second section, the wall heat-flux distribution, taken from experiments by Rose *et al.*, serves for comparison. Moreover a code-to-code comparison is performed with a recent numerical work[8] based on a finite volume method using the Roe flux-difference split scheme.
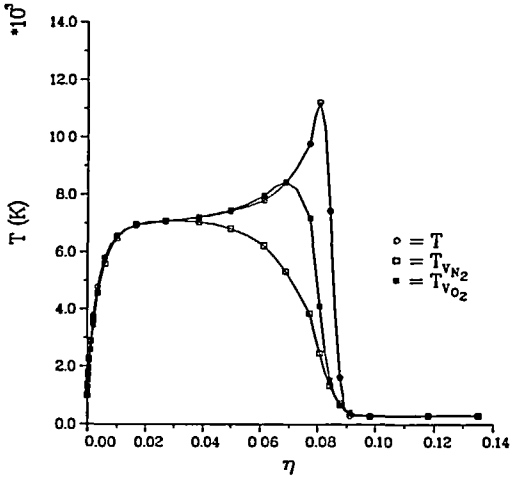
$-M_\infty = 15.35$

Figure 2 Stagnation streamline temperature distributions ($M_\infty = 15.35$)
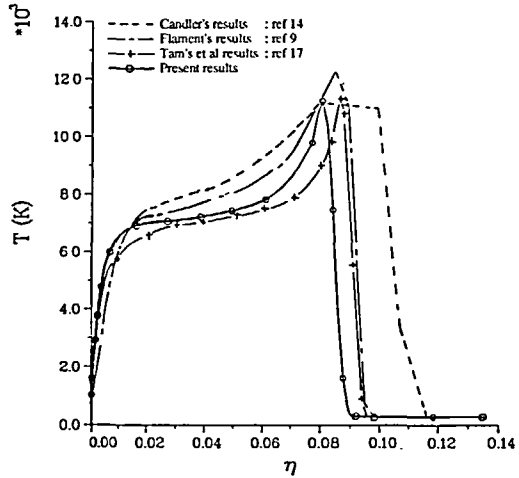

Figure 3 Comparison of stagnation streamline temperature distributions ($M_\infty = 15.35$)
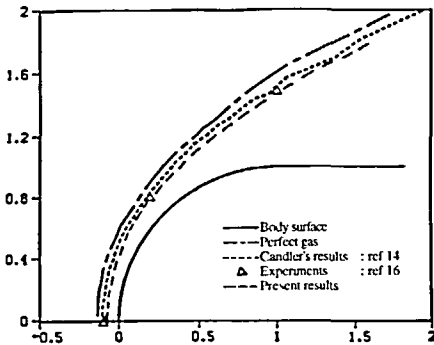

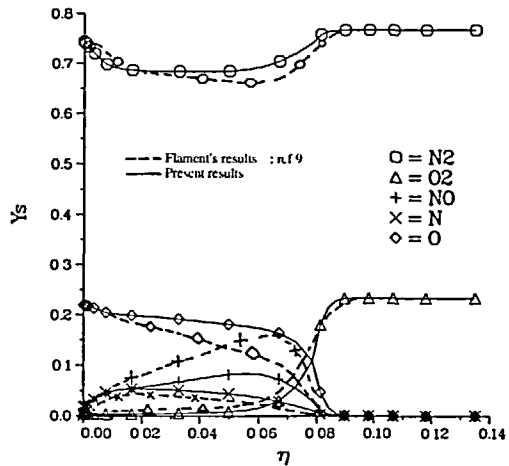*Figure 4* Comparison of shock standoff ($M_\infty = 15.35$)

Figure 5 Comparison of stagnation streamline species mass fractions distributions ($M_\infty = 15.35$)

This can has often been used in the literature[9,14,17] for code validation of chemical and thermal nonequilibrium flows. *Figure 2* shows the evolution of the translational and vibrational temperatures along the stagnation streamline. The vibrational non-equilibrium region of each diatomic species is clearly visible, and also the boundary layer in a thermal equilibrium state. In the core flow, the relaxation zone of O_2 is longer than that of N_2. The translational temperature profile is compared to those given by other authors in *Figure 3*. Some discrepancies can be noted. In the present computations, the thermal boundary layer is thinner also, a more pronounced plateau, and, finally, a shorter shock standoff distance is noticed. This last remark seems to be in agreement with experimental results, as shown in *Figure 4*, where Candler's results are also represented. The mass-fraction evolutions along the stagnation streamline are plotted in *Figure 5*, where the numerical results of Reference 9 are also plotted. The more pronounced differences concern NO and O evolutions and can be explained by the discrepancies on the temperatures as discussed previously.
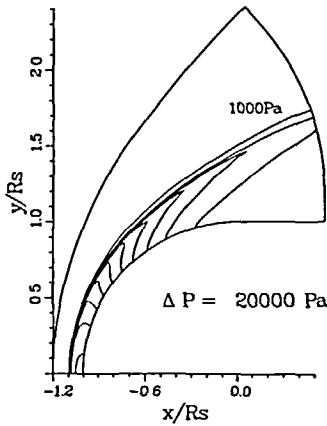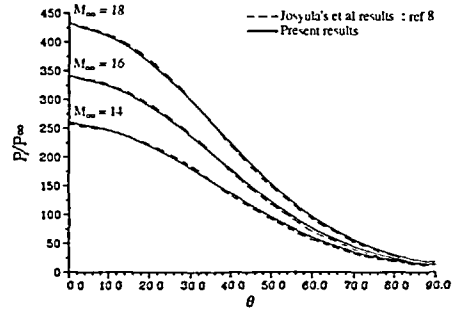
Figure 6   Pressure contours ($M_\infty = 15.35$)

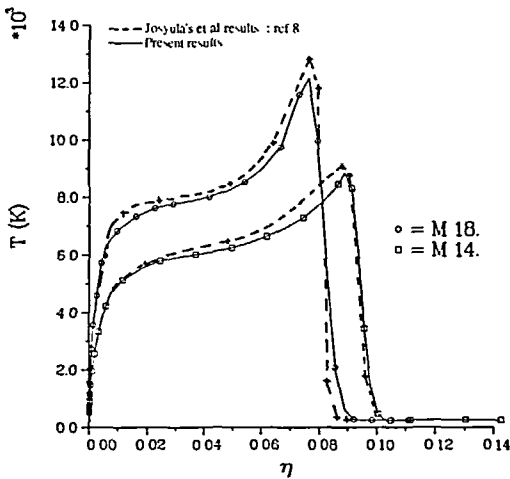Figure 7   Comparison of wall pressure profiles at different Mach numbers

Figure 8   Comparison of stagnation streamline temperature distributions
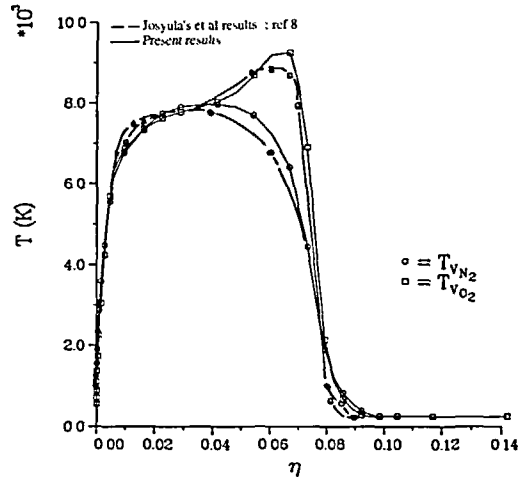

Figure 9   Comparison of stagnation streamline vibrational temperature distributions

One example of pressure isolines is drawn in *Figure 6*. With the help of these distributions, the position of the bow shock can easily be located.

$-M_\infty = 18, 16, 14$

Numerical results are discussed for three values of the freestream Mach number at an altitude of 37 km, where stagnation point heat transfer data are measured by Rose et al.[18]. These data are also used by Shang[8] in order to validate their numerical results. *Figure 7* shows the predicted surface pressure distributions for the three Mach numbers. Excellent agreement can be noted with the numerical results of Reference 8, which are also plotted. The wall pressure distributions do not seem affected by the choice of the numerical method and the vibrational model.

This code-to-code comparison goes on in *Figure 8*, where the translational temperature distributions along the stagnation streamline for two values of the Mach number ($M_\infty = 18$ and 14) are drawn. The shock standoff distance is about the same. The slight differences existing
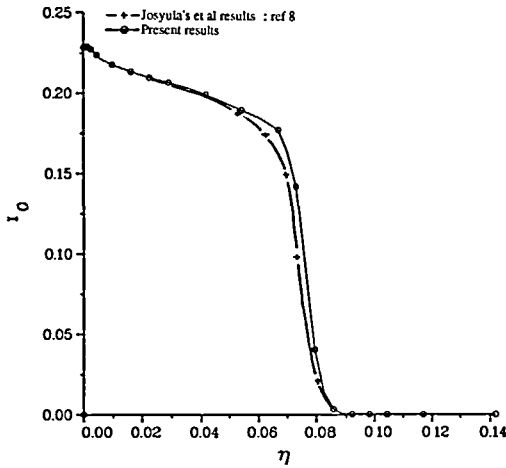
Figure 10   Comparison of stagnation streamline NO mass fraction distributions
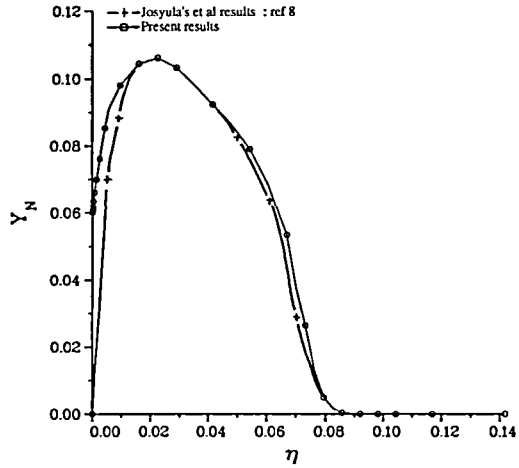

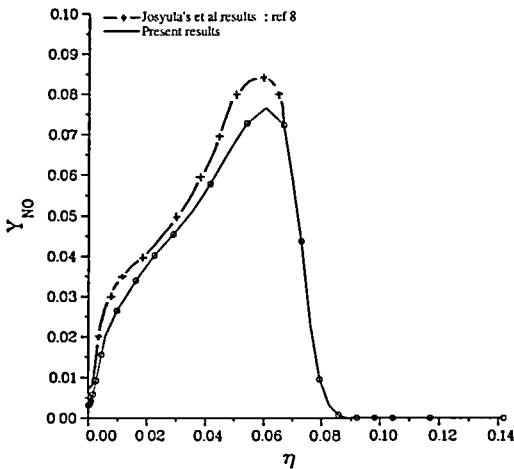Figure 11   Comparison of stagnation streamline O mass fraction distributions

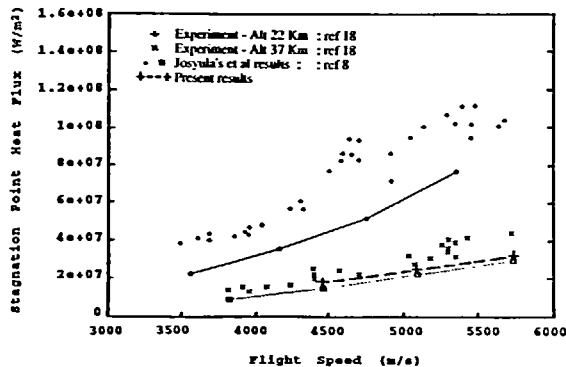Figure 12   Comparison of stagnation strealine N mass fraction distributions

Figure 13   Comparison of stagnation point heat flux distributions

between the two compuations can be explained by the choice of thermal equilibrium for the NO molecule in our case, the agreement is better at lower Mach number concerning the thermal boundary layer. Some slight discrepancies can also be noted in the vibrational temperature evolutions of N_2 and O_2 along the stagnation line, as seen in Figure 9.

The dissociation of diatomic species N_2 and O_2 behind the bow shock wave leads to apparition of the species O, N and NO. Figures 10, 11 and 12 show their mass-fraction evolutions along the stagnation streamline. By comparison with those obtained in References 8, a similar behaviour can be remarked. But lower values for the NO distribution, a rather good comparison for O and an important discrepancy of N in the boundary layer profile can be noticed. This last remark is perhaps coupled with the behaviour of NO within the boundary layer.

The stagnation point heat transfer, deduced from the present computations, is reported in Figure 13. This Figure, which contains experimental results of Rose et al. and computational ones by Josyula and Shang, has been taken from Reference 8. Our computed results follow
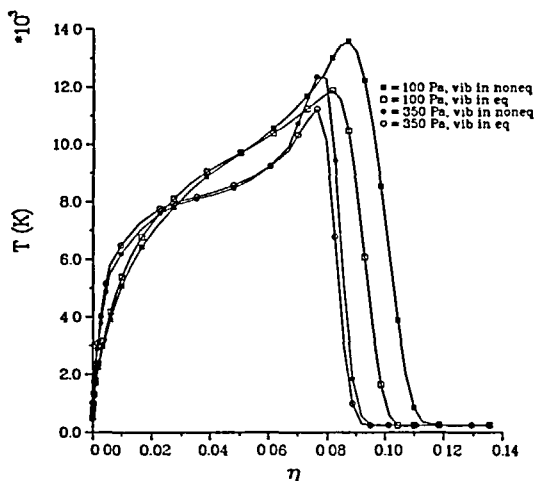
Figure 14 Stagnation streamline temperature distribution
at different upstream pressures

the trends of the experiments and are slightly higher than those obtained by Josyula and Shang, but they also underpredict the experiments. This discrepancy increases with the Mach number. It is may be due to the ionization effects.

At Mach number of 18, the addition of the vibrational non-equilibrium assumption does not sensibly modify the shock standoff distance obtained in equilibrium conditions. This distance tends to become Mach number-independent for this given upstream pressure ($P = 432$ Pa). But this remark is not valid if the pressure is decreased, for the same Mach number, as shown *Figure 14*. In this Figure the translational temperature distributions, for the vibrational equilibrium and non-equilibrium assumptions, are drawn for two lower upstream pressures respectively equal to 350 ($Re = 10,320$) and 100 *Pa* ($Re = 2950$). The shock standoff distance increases when the pressure decreases, and also the discrepancy of these distances is more pronounced between these two assumptions when the pressure decreases.

CONCLUSIONS

The chemical and vibrational non-equilibrium hypersonic air flow around a hemisphere-cylinder model has been simulated numerically by a finite-difference implicit method. The present results were compared with others computations in the same upstream conditions corresponding to available experimental data, and more particularly, with the recent numerical work of Josuyla and Shang. From these comparisons, some conclusions can be drawn:

(1) A good agreement is found for the wall pressure, as well as for the translational and vibrational temperature evolutions along the stagnation streamline.
(2) The thermal non-equilibrium of the NO molecule has a very slight effect on these evolutions.
(3) For the three tested Mach numbers, the computed wall heat flux are under the experimental ones when the Mach number increases. The ionization effect can play an important role in the wall heat transfer for the highest Mach number values.
(4) Some discrepancies are found on the mass-fraction of the N species within the boundary layer thickness, and on the influence of the thermal non-equilibrium assumption on the shock standoff distance when the Mach number increases.